Wesleyan University

A Clever Title

by

Jonas Powell
Class of 2019

A thesis submitted to the
faculty of Wesleyan University
in partial fulfillment of the requirements for the
Degree of Master of Arts

Middletown, Connecticut April, 2018

If people sat outside and looked at the stars each night,

I'll bet they'd live a lot differently.

—Calvin & Hobbes

Contents

Chapter 1

Analysis

Access to both spatially and spectrally resolved observations of protoplanetary disks offers a unique view into their chemical and physical characteristics, characteristics that we may discover through modeling. Modeling, in its essence, is the process of generating a synthetic image of what a disk with known physical characteristics (like disk radius, mass, and so on) would look like at a certain distance, inclination, and position angle relative to us. From that synthetic image, we may generate a synthetic set of visibilities, and then compare those visibilities to our observations. By iterating this process, we may generate many models with different parameter combinations and evaluate how well each resulting model disk matches our observations. Aggregating these results allows us to discover best-fit regions of parameter space, and thus make inferences about the nature of our sources based on those best-fit parameters.

In §1.1, we describe the basic equations and computational processes that generate the model disks. In §1.2, we describe how, once models are made, we may move through high-dimensional parameter space to identify regions of best-fit. Finally, in §1.3, we present the results of our fitting procedures.

1.1 Gas Model

Cail does way, way less for this stuff.

In this work, we use a gas model originally developed by Rosenfeld et al. (2012a, 2013 reference) and translated from IDL to Python by Flaherty et al (reference). The code develops its model in a two step process, using a few assumptions to decrease computational and mathematical complexity. The first half of the code is a ray-tracing routine. Ray tracing is a computational image-rendering process that involves tracing the paths that light rays take from emitting bodies, and simulating their interactions with the local environment (here, protoplanetary disks). The second step the code takes is executing a radiative transfer process. Radiative transfer simulates and describes the propagation of electromagnetic radiation through media and those media's absorptive, emitting, and scattering effects on that radiation.

1.1.1 Establishing Temperature, Density, and Velocity Profiles

One major assumption that this code leverages is that the disk is under local thermal equilibrium (LTE). This assumption allows for significant computational simplifications to be made, yielding significantly decreased computation time. This, in turn, offers us the chance to generate models quickly and thus explore parameter space more completely. While it is not clear whether the assumption of LTE is always a valid one in propluds, it has been shown to be appropriate for CO (Pavlyuchenkov et al. (2007) reference).

The second primary assumption that this code makes is that the motions of the disks' gas are described by a Keplerian velocity field with no vertical or radial components, given by

$$v(r) = \sqrt{\frac{GM}{r}};\ v_r = v_z = 0. \tag{1.1}$$

This assumption in the case that $M_{\rm disk} \ll M_\star$. Previous measurements of the disks' masses from continuum observations indicate that this is a valid assumption.

The two primary structures that concern us when parametrizing a model disk are the temperature and density structures. Here, we use the parametrization of disk temperature structure given by Dartois et al. (2003 reference) The temperature profile's radial component is given by a relatively simple power law, indexed by q, in T_a, while its vertical component is given by a more complicated sinusoid to simulate the temperature falloff with distance from midplane.

$$T_{\rm gas}(r,z) = \begin{cases} T_a + (T_m - T_a)\left[\cos\frac{\pi z}{2z_q}^{2\delta}\right] \text{ if } z > z_q \\ T_a \text{ if } z \leq z_q \end{cases} \tag{1.2}$$

where the atmospheric temperature and mid-plane temperatures are given by $T_a = T_{atm,150}(r/150\text{AU})^{-q}$ and $T_m = T_{mid,150}(r/150AU)^{-q}$. The height of the disk, controlled by z_q is assumed to have a radial distribution described by a power law, $z_q = z_{q,150}(r/150AU)^{1.3}$. Here we set δ to 1, though it can take on values between 1-2 (what is δ?).

Each disk's density structure is drawn from work by Lynden-Bell Pringle (1974) and Hartmann et al. (1998), in which they model a thin viscous accretion disk with a gas surface density profile given by a tapered power law,

$$\Sigma_{\text{gas}}(r) = \frac{M_{\text{gas}}(2-\gamma)}{2\pi R_c^2}\left(\frac{r}{R_c}\right)^{-\gamma}\exp\left[-\left(\frac{r}{R_c}\right)^{2-\gamma}\right] \tag{1.3}$$

where R_c is the radial extent of the gas disk, γ is a power law index, and M_{gas} is the total gas mass.

The use of an exponential radial decay rather than a sharply defined outer radius (i.e. the use of a tapered power law, rather than a truncated one) is chosen to reflect in part the structure's greater physical plausibility and in part because the structure has been shown to resolve apparent historical disagreements between continuum and gas emission observations,

At these early stages of a circumstellar disk's life, the disk is composed almost entirely of gas; the canonical dust-mass percentage in proplyds is less than 1%. Consequently, we may safely approximate the disk's gas mass as $M_{\text{gas}} = M_{\text{disk}}$.

Drawing on these profiles, we may now find a solution for the disk's radial density profile by integrating the equation of hydrostatic equilibrium,

$$-\frac{\partial \ln \rho_{\text{gas}}}{\partial z} = \frac{\partial \ln T_{\text{gas}}}{\partial z} + \frac{1}{c_s^2}\left[\frac{GMz}{(r^2+z^2)^{3/2}}\right]. \tag{1.4}$$

Here c_s is the local sound speed, given by

$$c_s = \sqrt{\frac{k_B T_{\text{gas}}}{\mu m_H}}, \tag{1.5}$$

and μm_H is the mean molecular weight (of a specific molecule? Hydrogen? Idk).

Modifications are made to this density profile in two cases. At sufficiently low temperatures, molecules will condense out of the gas phase. The mid-plane of the disk is sufficiently cold to prompt this behavior. We may simulate this behavior by dropping the gas density by a factor of 10^{-18} wherever the temperature falls below some characteristic freeze-out temperature, T_{FO}, a temperature which is molecule-specific. In this work, we use $T_{FO} = 19$K for HCO^+, CO, and CS, and $T_{FO} = 60$K for HCN (why is this again?). Conversely, at the disk's upper surface, photodissociation by stellar radiation dominates, so we implement a decrease in density wherever the hydrogen column density at the disk's surface falls below a characteristic value (for HCO^+, CO, and CS, this value is $1.3 \times 10^{-21}\text{cm}^{-2}$, whereas for HCN it is $9.5 \times 10^{-21}\text{cm}^{-2}$ (again, why, and also what's the other column density value that I feed into the model?)). The temperature and density structure of a typical proplyd is shown in Fig 1.1.

Having characterized our model disk's temperature and density profiles, we may now calculate its velocity profile, adding a term to Eq. 1.1, which describes pure Keplerian rotation, to account for the force induced by the pressure gradient we introduced above:

$$\frac{v_\phi^2}{r} = \sqrt{\frac{GM}{r}} + \frac{1}{\rho_{\text{gas}}}\frac{\partial P_{\text{gas}}}{\partial r}. \tag{1.6}$$

(Velocities are still restricted to being purely angular, with no radial or vertical components).

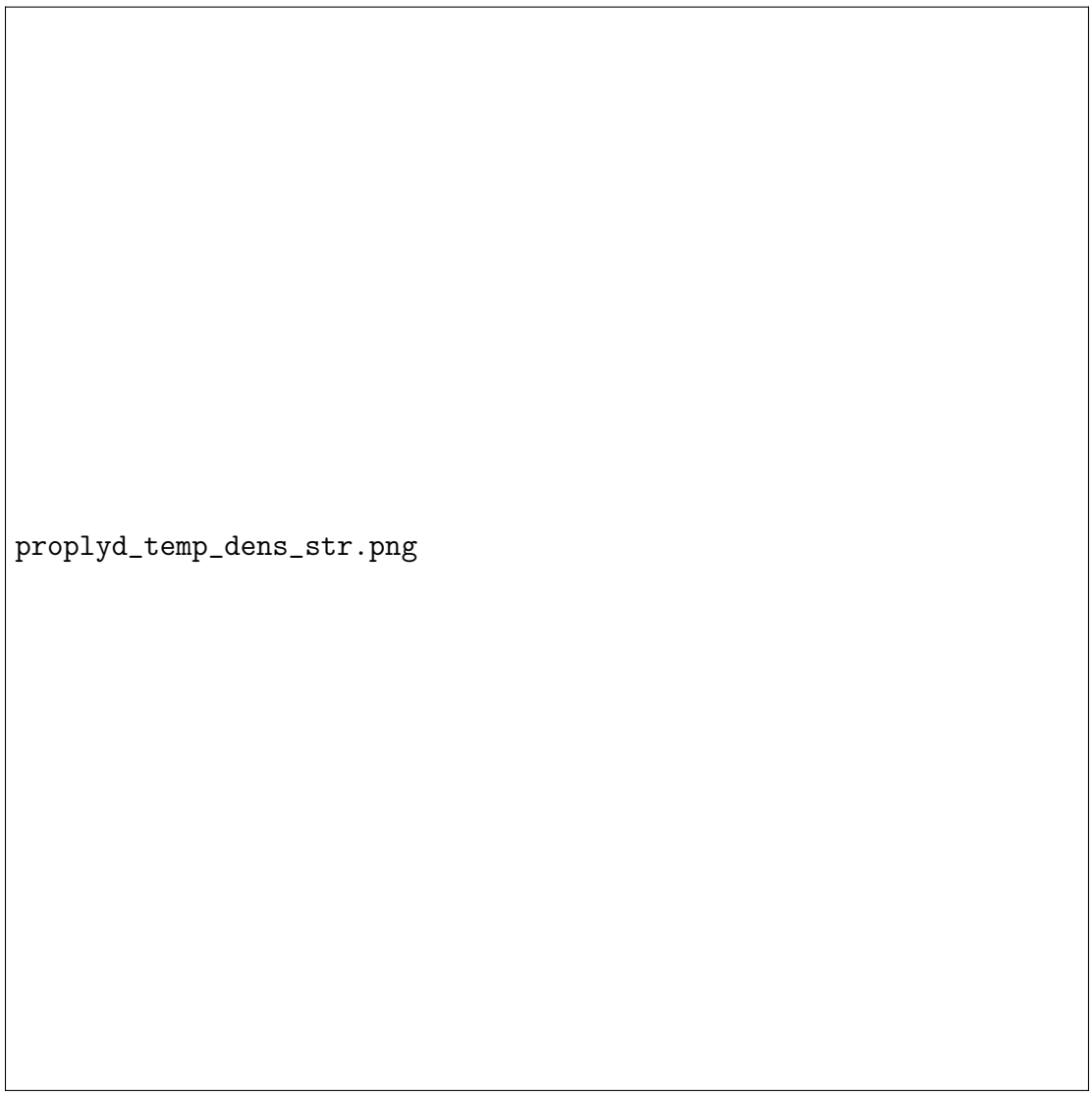

Figure 1.1: A disk structure plot.

1.1.2 Radiative Transfer

Having now established our model disk's physical structure through temperature, density, and velocity profiles, we may begin generating an image of the disk by performing radiative transfer on this structure. To do so, we calculate the specific intensity by integrating the equation of radiative transfer:

$$I_\nu = \int_0^\infty K_\nu(s)\ S_\nu(s)\ e^{-\tau_\nu(s)}\ ds, \tag{1.7}$$

where $K_\nu(s)$ is the absorption coefficient, $\tau_\nu(s)$ is the optical depth, and $S_\nu(s)$ is the source function. Since disks emit as blackbodies, we use the Planck function, $B_\nu(T)$, as the source function. The optical depth, $\tau_\nu(s)$, along a line of sight is given by

$$\tau_\nu(s) = \int_0^s K_\nu(s')ds' \tag{1.8}$$

The absorption coefficient, $K_\nu(s)$, is given by the product of the level populations of the molecule being observed ($n_l(s)$), the absorption cross-section of that molecule ($\sigma_n(s)$), and something else that Sam didn't define ($u(s)$), as $K_\nu(s) = n_l(s)\ \sigma_n(s)\ u(s)$.

Should I really keep going with these equations?

1.1.3 Generating a Model

We now have the ability to generate a model disk, first by calculating its physical structures (in radial temperatures, densities, and velocities), and then by performing radiative transfer on that structure. The resulting synthetic image can be tuned to best fit our data by varying any of the large number of input parameters (given in a table maybe).

Since the model disk is fully defined at every point in both physical and velocity space, we may choose our spatial and spectral resolutions arbitrarily. We set our spectral resolution to match that of our observation, while we let the spatial resolution be $\sim 1/10$ the size of the synthesized beam. This resolution is high enough to avoid sampling artifacts when we simulate interferometric observations of the image.

- Hanning smoothing: This reduces the ringing in the frequency domain caused by Fourier transforming sharp features. - Simulate observations using the Miriad task `uvmodel` with `options=replace`, drawing on the visibilities from our observed data. The uvmodel task calculates the FT of the image then samples it using the UV tracks of our observations. This resulting visibilities are how our model image would look were it observed using the same array configuration as the one used to gather the data. - Then use the χ^2 statistic as a goodness of fit metric to compare the data and model in the visibility domain. We make this calculation in the visibility domain, rather than the image domain, so that the resulting χ^2 value is not influenced by artifacts generated in the imaging process.

In this project, we fit for the following parameters:

- Atmospheric Temperature (T_{atms}): The temperature of the disk somewhere.

- Outer Radius (R_{out}: The outer radius of the molecule under observation in the disk. This can vary by line, thanks to different excitation temperatures and densities.

- Radial Temperature Power Law Index (T_{qq}): The exponent of the power law that governs the disk's radial temperature structure, i.e. $T(r) \propto r^{T_{qq}}$. Since disk B is unresolved and thus changing this would be meaningless, we fix T_{qq} at a typical value of -0.2.

- Relative Molecular Abundance ($X_{\rm mol}$): The relative molecular abundance indicates the fractional abundance of the molecule under observation relative to the H_2 abundance. We fit for $X_{\rm mol}$ for our HCO^+, HCN, and CS models, but fix it at the literature value of 10^{-4} for our CO fitting.

- Log Disk Mass ($\log M_{\rm disk}$): The base-10 logarithm of each disk's mass. We fit for $\log M_{\rm disk}$ only in the CO data, where $X_{\rm mol}$ is fixed. In all other lines, we fix it at

- Inclination (i): The disk's inclination angle.

- Position Angle (PA): The disk's position angle.

A selection of the remaining parameters, which we leave fixed, are summarized in Table 1.1.3.

Fixed Parameters **Not convinced that this is necessary. Incomplete at the moment.**

v_{sys}	Systemic velocity	The line-of-sight velocity of the disk.
$\Delta\delta, \Delta\alpha$	Position Offset	Each disk's distance from the center of the field of view.
$M_\star$	Stellar Mass	The masses of each disk, from Someone et al (1900 refere
v_{sys}	Systemic velocity (km/s)	The line-of-sight velocity of the disk.
d	Distance	The distance to the sources, from Gaia.

1.2 Exploring Parameter Space

Now that we have the tools available to generate synthetic images that are tuneable across a large number of parameters, we must decide how best to move through that large parameter space to find a best-fit region. To do so, we use two methods.

1.2.1 Grid Search

The first, and perhaps most intuitive, way to move through this parameter space is using a simple grid search. A grid search involves manually assembling lists of values to try for each parameter and then generating models and calculating the resulting χ^2 value for every possible combination of parameters in those lists. A best-fit value is recovered by simply finding the point in that n-dimensional grid that yielded the best χ^2, and then either calling that position in parameter space a best-fit location or then defining a finer grid around that point and repeating the process until an acceptable resolution has been reached. Benefits of grid search include its relatively straightforward nature (the the consequent simplicity of implementation) and its usefullness as a diagnostic tool, since very specific regions of parameter space may be sampled with the manual entry of positions to

test. However, it is a relatively simple method and leaves room for improvement.

1.2.2 Markov Chain Monte Carlo

Markov Chain Monte Carlo (MCMC) algorithms offer us a way to both sample the probability distribution of a complex parameter space (much like a grid search), but offer an improvement over grid search by yielding the posterior probability distribution of each point, allowing us to characterize the uncertainty associated with each best-fit value with error bars. We use an affine-invariant formulation of the MCMC algorithm described by Goodman & Weare (2010 reference) and implemented in the Python package emcee by Foreman-Mackey et al 2013 (reference).

MCMC routines sample the probability distribution of a given n-dimensional parameter space by deploying an army of "walkers." Each walker begins at some initial position, evaluates the χ^2 value of that point, and then proposes moving to a new position in parameter space according to a Gaussian probability distribution centered at the current point and decaying with distance (so that nearer points are preferentially - but not necessarily - selected). The χ^2 value of this new position - or "step" - is then evaluated, and is either accepted (the walker moves to that position) or rejected (the walker remains where it is and repeats the new-step proposal process) with probability $p = \exp\left[(\chi^2_{\rm current} - \chi^2_{\rm new})/2\right]$ (is this only for Metropolis Hastings?). This function indicates that if the proposed step yields a better fit (a lower χ^2 value) than the current position, $p > 1$ and the step is accepted. However, if proposed step results in a worse fit, there is still a non-zero chance that the step is accepted, proportional to how much worse it is. This willingness to accept an increased χ^2 value allows the walker to avoid

becoming trapped in local minima. The list of steps taken by each walker and their accompanying χ^2 values are compiled into the "chain" part of Markov Chain Monte Carlo. It has been demonstrated (reference?) that a walker's desire to remain in a location is proportional to the local probability density, meaning that we may infer uncertainties in our fits from the density of walker steps taken in a region.

We may introduce boundaries to the parameter space explored by our walkers using "priors." These priors are manually set, and allow us to save time by restricting the walkers' motions into regions that we know a priori to be implausible fits. The priors used for this project are given in Table 1.2.2.

Priors for Fit Parameters **Probably have to make this long format.**

Disk	R_{out}	T_{atms}	i	PA	X_{mol}	$\log M_{disk}$
Tqq						
A	(10, 1000)	(0, 1000)	(0, 90)	(0, 360)	(-13, -3)	(-2.5, 0)
(-3, 3)						
B	(10, 1000)	(0, 1000)	(0, 90)	(0, 360)	(-13, -3)	Fixed
Fixed						

We may visualize our results using corner plots. Corner plots allow high-dimensional space to be visualized in two dimensions by taking slices across each pair of axes and showing the density of samples drawn in that slice. In each of these slices, a perfectly certain fit would appear as a very tight Gaussian - the sample density around the best fit would be extremely high and low everywhere else - while conversely, higher uncertainties are shown by a wide spread of samples around the central point. Degeneracies between parameters can be seen in non-point-like distributions of samples (i.e. some correlation between dimensions). A

corner plot is shown in Fig 1.2.

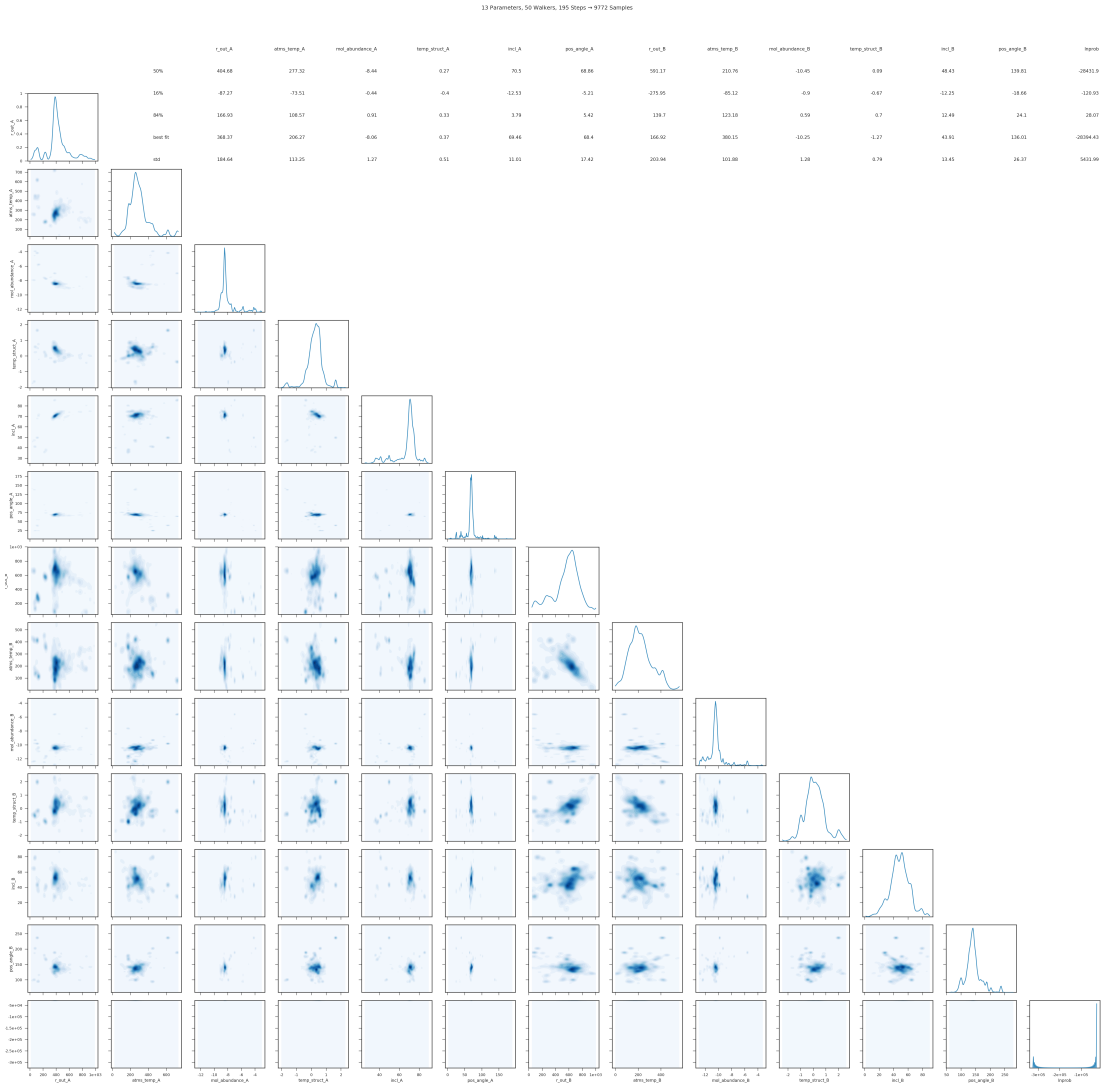

Figure 1.2: A corner plot.

1.3 Fitting Procedure

With our model-making and fitting procedures established, we may now consider the actual process.

- Fits were made to data with cut baselines (see section something for a dis-

cussion on cloud contamination)

Before starting any sort of fitting, we first had to locate the disk in $[\alpha, \delta, v]$ space. To do so, we fixed all disk parameters at hand-selected, ballpark-reasonable values and ran a grid search over RA/dec offsets and systemic velocities for each disk, using final grid resolutions that corresponded to the beam width and spectral resolution, respectively. In this process, we fit only the HCO^+ line due to its high signal-to-noise ratio. We confirmed positional offsets using some tool in `CASA`. The results of these fits are reported in Table 1.3.

XYV Offsets **Looking bad now, will get better later.**

	α	δ	v	
Disk A	0.0002	0.082	10.0	
Disk B	-1.006	-0.3	10.75	

Should probably put uncertainties into these reports. Also probably don't need a subsection for every line, just the important ones. Will depend on results.

1.3.1 CO (3-2) Fit

Starting with CO to get disk mass.

Best fit values are reported in Table 1.3.1

CO (3-2) Best-Fit Paramers

	R_{out}	T_{atms}	i	PA	$\log M_{disk}$	Tqq
Disk A	1	1	1	1	1	1
Disk B	1	1	1	1	1	1

1.3.2 HCO^+ (4-3) Fit

Then the rest of them, probably HCO next because low contamination.

Best fit values are reported in Table 1.3.2

HCO^+ (4-3) Best-Fit Paramers

	R_{out}	T_{atms}	i	PA	$\log M_{disk}$	Tqq
Disk A	1	1	1	1	1	1
Disk B	1	1	1	1	1	1

1.3.3 HCO^+ (4-3) Fit

Then the rest of them, probably HCO next because low contamination.

Best fit values are reported in Table 1.3.3

HCN (4-3) Best-Fit Paramers

	R_{out}	T_{atms}	i	PA	$\log M_{disk}$	Tqq
Disk A	1	1	1	1	1	1
Disk B	1	1	1	1	1	1

1.3.4 CS (7-6) Fit

Blah blah blah Best fit values are reported in Table 1.3.4

CS (7-6) Best-Fit Paramers

	R_{out}	T_{atms}	i	PA	$\log M_{disk}$	Tqq
Disk A	1	1	1	1	1	1
Disk B	1	1	1	1	1	1

Bibliography

Collaboration, G. 2016, Astronomy & Astrophysics, 595, A1, arXiv: 1609.04153

Collaboration, G., Brown, A. G. A., Vallenari, A., Prusti, T., de Bruijne, J. H. J., Babusiaux, C., & Bailer-Jones, C. A. L. 2018, Astronomy & Astrophysics, 616, A1, arXiv: 1804.09365

Factor, S. M., et al. 2017, The Astronomical Journal, 153, 233, arXiv: 1704.01970

Goodman, J., & Weare, J. 2010, Communications in Applied Mathematics and Computational Science, 5, 65

Mann, R. K., et al. 2014, The Astrophysical Journal, 784, 82, arXiv: 1403.2026

Mann, R. K., & Williams, J. P. 2009, The Astrophysical Journal, 699, L55

Ricci, L., Robberto, M., & Soderblom, D. R. 2008, The Astronomical Journal, 136, 2136

Ricci, L., Testi, L., Williams, J. P., Mann, R. K., & Birnstiel, T. 2011, The Astrophysical Journal, 739, L8

RJ Sault, MCH Wright, R. S. H. P. J. H. P. T. 1995, ASP Conf. Ser., 77, 433

Sault, R. J., Teuben, P. J., & Wright, M. C. H. 2006, arXiv:astro-ph/0612759, arXiv: astro-ph/0612759

Smith, N., Bally, J., Licht, D., & Walawender, J. 2005, The Astronomical Journal, 129, 382

Williams, J. P., et al. 2014, The Astrophysical Journal, 796, 120, arXiv: 1410.3570